A&A 384, 383–392 (2002)
DOI: 10.1051/0004-6361:20011830

Astronomy & Astrophysics

A deep Hα survey of galaxies in the two nearby clusters Abell 1367 and Coma*

The Hα luminosity functions

J. Iglesias-Páramo[1], A. Boselli[1], L. Cortese[2], J. M. Vílchez[3], and G. Gavazzi[2]

[1] Laboratoire d'Astrophysique de Marseille, Traverse du Siphon – Les Trois Lucs, 13376 Marseille, France
e-mail: jorge.iglesias@astrsp-mrs.fr;alessandro.boselli@astrsp-mrs.fr
[2] Università degli Studi di Milano – Bicocca, P.zza delle scienze 3, 20126 Milano, Italy
e-mail: giuseppe.gavazzi@mib.infn.it; luca.cortese@mib.infn.it
[3] Instituto de Astrofísica de Andalucía (CSIC), Granada, Spain
e-mail: jvm@iaa.es

Received 13 November 2001 / Accepted 14 December 2001

Abstract. We present a deep wide field Hα imaging survey of the central regions of the two nearby clusters of galaxies Coma and Abell 1367, taken with the WFC at the INT 2.5 m telescope. We determine for the first time the Schechter parameters of the Hα luminosity function (LF) of cluster galaxies. The Hα LFs of Abell 1367 and Coma are compared with each other and with that of Virgo, estimated using the B band LF by Sandage et al. (1985) and a $L(\mathrm{H}\alpha)$ vs. M_B relation. Typical parameters of $\phi^* \approx 10^{0.00\pm0.07}$ Mpc^{-3}, $L^* \approx 10^{41.25\pm0.05}$ erg s^{-1} and $\alpha \approx -0.70 \pm 0.10$ are found for the three clusters. The best fitting parameters of the cluster LFs differ from those found for field galaxies, showing flatter slopes and lower scaling luminosities L^*. Since, however, our Hα survey is significantly deeper than those of field galaxies, this result must be confirmed on similarly deep measurements of field galaxies. By computing the total SFR per unit volume of cluster galaxies, and taking into account the cluster density in the local Universe, we estimate that the contribution of clusters like Coma and Abell 1367 is approximately 0.25% of the SFR per unit volume of the local Universe.

Key words. atlases – galaxies – ISM: HII regions – galaxies: clusters: individual: Abell 1367; Coma; Virgo

1. Introduction

The strong morphology segregation observed in rich clusters of galaxies (Dressler 1980) testifies to the fundamental role played by the environment on the evolution of galaxies. Which physical mechanisms are responsible for such transformations is however still a matter of debate. Several processes might alter the evolution of cluster galaxies. Some of them refer to the interaction of the galaxies with the intracluster medium (Gunn & Gott 1972) and others account for the effects of gravitational interactions produced by the gravitational potential of the cluster (Merritt 1983) or by galaxy-galaxy interactions (Moore et al. 1996, 1998, 1999). All these mechanisms can produce strong perturbations in the galaxy morphology with the formation of tidal tails, dynamical disturbances which appear as asymmetries in the rotation curves (Dale et al. 2001) and significant gas removal (Giovanelli & Haynes 1985; Valluri & Jog 1990).

Some of these processes are expected to produce changes in the star formation rates of galaxies in clusters. Several studies have addressed the issue of the influence of the cluster environment on the SFR of disk galaxies, however no agreement has been established so far: while some authors proposed similar or even enhanced star formation in cluster spirals than in the field (Donas et al. 1990, 1995; Moss & Whittle 1993; Gavazzi & Contursi 1994; Moss et al. 1998; Gavazzi et al. 1998; Moss & Whittle 2000), some others claim quenched SFRs in cluster spirals (Kennicutt 1983; Balogh et al. 1998; Hashimoto et al. 1998). This discrepancy could arise from non-uniformity of the adopted methods (UV vs. Hα vs. [OII] data) or from real differences in the studied clusters (Virgo, Coma, Abell 1367, clusters from Las Campanas Redshift Survey, clusters at $z > 0.18$).

In particular, an enhanced fraction of spirals with circumnuclear Hα emission was found in the highest density regions of some nearby clusters (Moss et al. 1998; Moss & Whittle 2000), whereas no such difference was found for

Send offprint requests to: J. Iglesias-Páramo,
e-mail: jorge.iglesias@astrsp-mrs.fr

* Appendix A is only available in electronic form at http://www.edpsciences.org

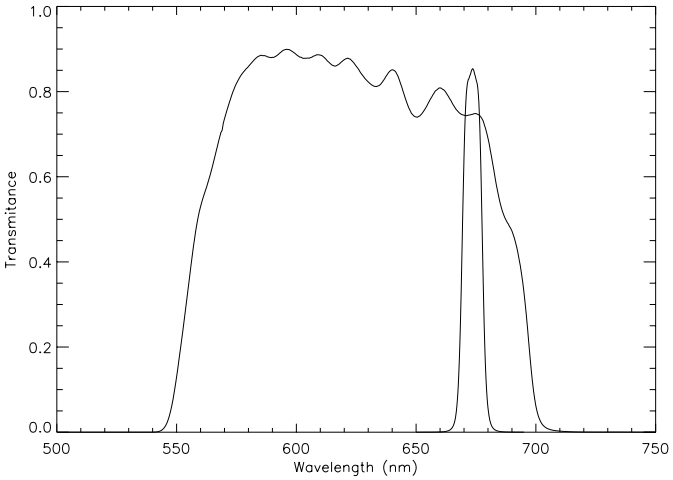

Fig. 1. Transmitance of the filters used for the observations.

galaxies with diffuse emission. The compact Hα emission seems associated with ongoing interactions of galaxies, but numerical simulations by Bekki (1999) showed that mergers between clusters and subclusters might produce central starbursts in cluster spirals.

Existing studies of the Hα properties of galaxies in clusters suffer from various biases: the photoelectric data by Kennicutt et al. (1984) and Gavazzi et al. (1991, 1998) are based on samples of galaxies selected on the basis of their optical properties, independent of their Hα properties. On the other hand, the objective-prism surveys by Moss et al. (1988, 1998) and Moss & Whittle (2000) are Hα selected but they are too shallow to allow a determination of the Hα luminosity function as deep as desired.

With the aim of obtaining a reliable determination of the current SFR in nearby clusters of galaxies and to study the spatial distribution of the star formation regions, we undertook a deep imaging survey of a one degree × one degree area of the Coma and Abell 1367 clusters.

Our work provides the first deep and complete study of galaxies in clusters based on their Hα emission properties.

This paper is arranged as follows: Sect. 2 contains a description of the observations, of the data reduction and the detection procedures. The Hα data are presented in Sect. 3. The Hα luminosity function and a brief discussion of the contribution of both clusters to the local star formation rate density are presented in Sect. 4. Conclusions are presented in Sect. 5. Comments on the most interesting objects as well as the Hα images of the detected galaxies are given in the Appendix.

2. Observations and data reduction

The observations were carried out with the Wide Field Camera (WFC) at the Prime Focus at the INT 2.5 m telescope located at Observatorio de El Roque de los Muchachos (La Palma), on April 26th and 28th 2000, under photometric conditions. The average seeing ranged from 1.5 to 2 arcsecs during both nights. Given the mean velocity of the galaxies in the two clusters under study, $6555 \pm 684\,\mathrm{km\,s^{-1}}$ and $6990 \pm 821\,\mathrm{km\,s^{-1}}$ for Abell 1367 and Coma respectively[1] (Fadda et al. 1996), the narrow-band [SII] filter ($\lambda_0 = 6725$ Å, $\delta\lambda \approx 80$ Å) was used to isolate the Hα line and the r' Sloan-Gunn broad-band filter ($\lambda_0 = 6240$ Å, $\delta\lambda \approx 1347$ Å) to recover the continuum. Figure 1 shows the transmitance profiles of both filters. Given the width of the [SII] filter, the [NII]λλ6548, 6584 Å lines are included in the high transmitance pass-band of this filter, so in what follows we will refer to the combined Hα + [NII] flux and equivalent width, as Hα flux and equivalent width respectively.

The WFC is composed of a science array of four thinned AR coated EEV 4 K×2 K devices, plus a fifth acting as autoguider. The pixel scale is 0.333 arcsec pixel^{-1}, giving a total field of view of about 34×34 arcmin^2. Given the arrangement of the detectors, a square area of about 11×11 arcmin^2 is lost at the top right corner of the field. The top left corner of detector #3 is also lost because of filter vignetting.

Four fields near the center of each cluster were observed. Three different exposures, slightly dithered to remove cosmic rays, were obtained for each position in each filter, except for the second exposure of the Coma cluster where only one exposure per filter was obtained. Figure 2 shows our surveyed area. Our observations cover mainly the North-East region of the Coma cluster as described by Colless & Dunn (1996), coinciding with the central part of the Godwin catalog of the Coma cluster (Godwin et al. 1983). One of our fields of Abell 1367 (number 1 in Fig. 2) is not covered by the Godwin catalog (Godwin & Peach 1982). For comparison the X-ray contour maps of the two clusters (White et al. 1993 for Coma, and Donnelly et al. 1998 for Abell 1967) are plotted in the figure. The galaxies detected in Hα are marked with filled dots. The diary of the observations is presented in Table 1.

The data reduction was carried out using standard tools in the IRAF[2] environment. The astrometric solution was found with the USNO[3] catalog of stars. The accuracy of this solution was found to be better than 3 arcsecs throughout the frames. Several exposures of standard spectrophotometric stars were taken during both nights. The chip-to-chip differential responses were derived by direct comparison of the photometry measured for the objects, non-saturated stars and galaxies, present in the overlapping regions. Zero-points and extinction coefficients were derived from the calibration equations. Overall, our photometric uncertainty is less than 10%.

In order to properly subtract the continuum from the Hα frames, we scaled the counts of the continuum frames until (unsaturated) stars and elliptical galaxies reached

[1] For Abell 1367, we use the average of the redshifts reported in this paper.

[2] Image Reduction and Analysis Facility, written and supported at the National Optical Astronomy Observatory.

[3] United States Naval Observatory.

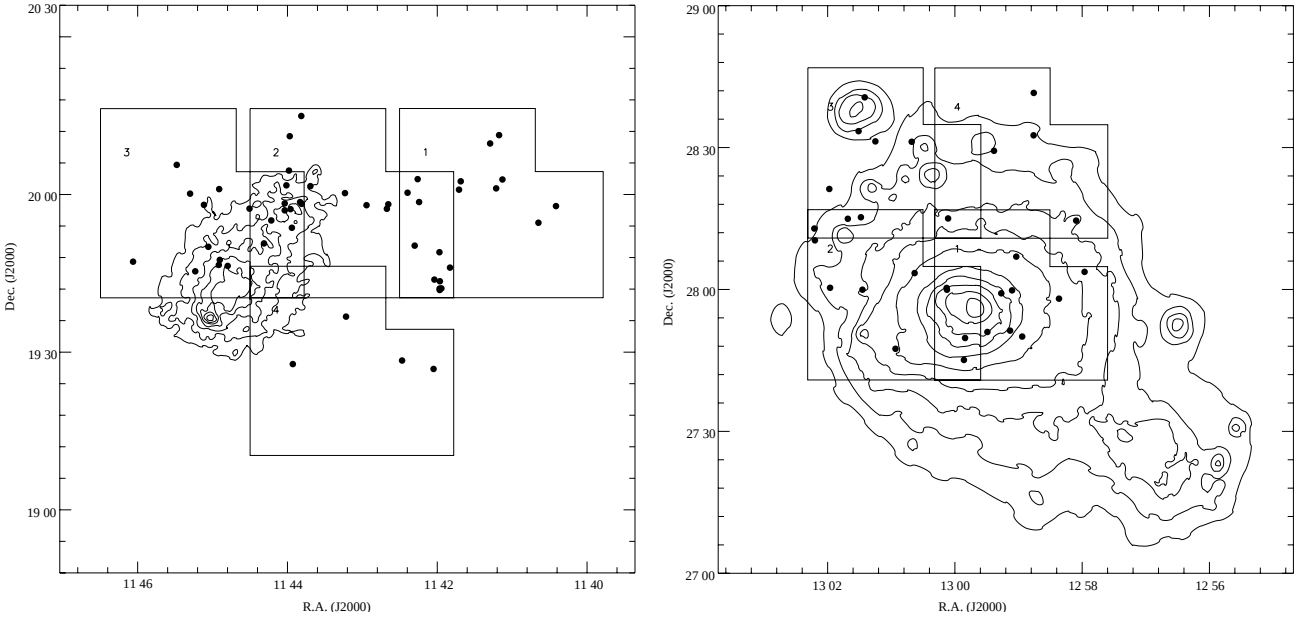

Fig. 2. Projected positions of our exposures in the Abell 1367 (left plot) and Coma (right plot) clusters. Superimposed contours correspond to the X-ray maps from Donnelly et al. (1998) and White et al. (1993) respectively. Filled dots represent the galaxies showing Hα emission.

an average Hα + [NII] equivalent width of 0 Å. The net Hα + [NII] photometry of the selected galaxies was performed using the QPHOT command of the APPHOT package in IRAF. Aperture photometry was carried out, in both the ON-band and continuum frames, for each galaxy and subtracted to get the net Hα + [NII] fluxes.

3. Object selection

We made extensive use of the NASA Extragalactic Database (NED) to search for known galaxies in the area covered by the observations. We measured the Hα + [NII] fluxes for all galaxies with known radial velocities, thus up to $r' \approx 15.5$ for Abell 1367 and $r' \approx 16.5$ for Coma.

The narrow band filter used did not cover the whole velocity interval of the clusters. In order to avoid large uncertainties in the determination of fluxes and equivalent widths, we measured only galaxies for which the filter transmitance was larger than 0.5.

Visual inspection of the net Hα + [NII] frames allowed us to identify faint galaxies with non-negligible net Hα + [NII] emission. For these galaxies, there is no estimate of their velocities in NED. A population of faint galaxies ($r' \geq 17.2$) showed up, most of them belonging to Abell 1367. Their Hα+ [NII] fluxes are low ($-15.53 < \log F(\mathrm{H}\alpha + [\mathrm{N\,II}]) < -13.83$ erg s^{-1} cm^{-2}) but their Hα equivalent width is in the range $9 < EW(\mathrm{H}\alpha + [\mathrm{N\,II}]) < 418$ Å. The search was performed for all objects visible on the NET-frames, but, in order to avoid spurious detections, we considered only objects with $F(\mathrm{H}\alpha + [\mathrm{N\,II}])/\sigma_{\mathrm{flux}} > 5$ as reliable detections (see Col. 9 of Tables 4 and 5 for the definition of σ_{flux}). Since for some of them, their redshift is unknown, both the Hα fluxes and equivalent widths were computed assuming that their velocity coincides with the average velocity of the cluster[4,5].

Table 1. Journal of the observations.

Field	RA (J2000)	Dec. (J2000)	Exp. s	Filter
		26th April 2000		
Coma 1	12:59:24.75	+27:58:49.89	3×1200	[SII]
			3×300	r'
Coma 2	13:01:24.45	+27:58:52.12	1200	[SII]
			300	r'
		28th April 2000		
Coma 3	13:01:24.26	+28:28:52.12	3×1200	[SII]
			3×300	r'
Coma 4	12:59:24.57	+28:58:49.89	3×1200	[SII]
			3×300	r'
		26th April 2000		
A1367 1	11:41:35.83	+19:58:21.44	3×1200	[SII]
			3×300	r'
A1367 2	11:43:35.61	+19:58:20.73	3×1200	[SII]
			3×300	r'
		28th April 2000		
A1367 3	11:45:35.40	+19:58:20.10	3×1200	[SII]
			3×300	r'
A1367 4	11:43:35.56	+19:28:20.73	3×1200	[SII]
			3×300	r'

[4] The transmitance peak of the filter is 0.85, and the transmitance for the Hα lines at the averages velocities of both clusters corresponds to 0.82 and 0.76 for Coma and Abell 1367 respectively.

[5] Contamination due the Hβ or [OIII] emission lines of background objects is not important. For some of these objects the redshift was measured and only less than 10% were found to be non members of the cluster.

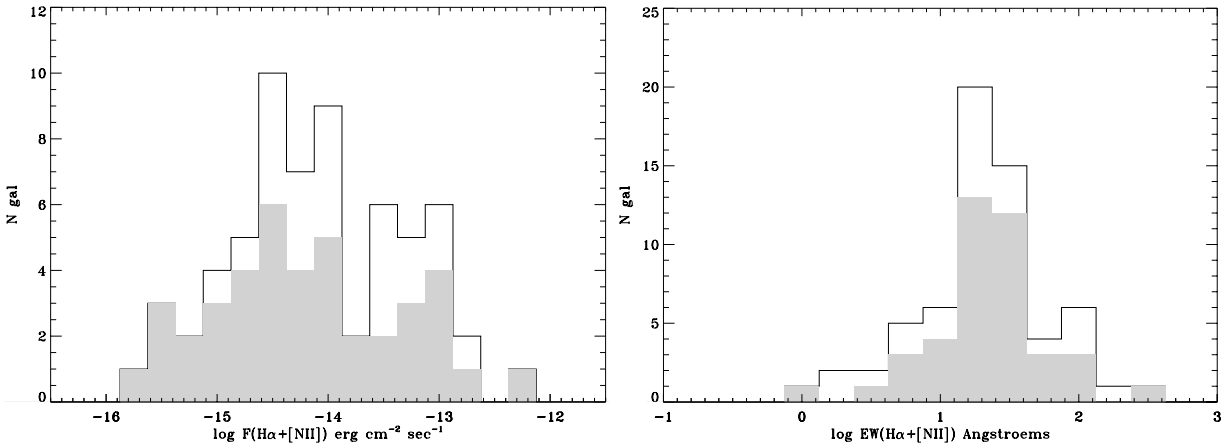

Fig. 3. Histograms of the Hα fluxes (left) and equivalent widths (right) of the emitting galaxies. Shaded bins correspond to the galaxies in Abell 1367.

In total 41 and 22 Hα emitting galaxies were detected in Abell 1367 and Coma respectively. These are listed in Tables 4 and 5, arranged as follows:

- *Column 1*: galaxy designation.
- *Column 2*: CGCG name (Zwicky et al. 1961-1968).
- *Column 3*: other source designation.
- *Columns 4, 5*: celestial coordinates (J2000).
- *Column 6*: radial velocity in km s^{-1}. Galaxies flagged with † are those detected in Hα but with unknown redshift. For these objects, the mean velocity of the cluster was adopted. Galaxies flagged with †† are those for which a spectroscopic follow-up was carried out in order to measure their redshifts (Gavazzi et al. 2002, in prep.).
- *Column 7*: magnitude in the r' band.
- *Column 8*: Log of the Hα+[NII] flux, in erg s^{-1} cm^{-2}.
- *Column 9*: error ($\sigma_{\rm flux}$) of the Hα+[NII] flux. The uncertainty includes three contributions: the Poisson photon counts error, the uncertainty on the background and the photometric uncertainty, which is assumed as 10% of the net flux. These errors were determined separately on the ON and OFF-band frames, and combined using the standard error propagation.
- *Column 10*: Hα+[NII] equivalent width in Å.
- *Column 11*: error in the Hα+[NII] equivalent width, computed similarly to $\sigma_{\rm flux}$ (Col. 9) except that the error on the absolute flux scale does not affect the equivalent width.

Figure 3 shows the histograms of Hα fluxes and equivalent widths of the emitting galaxies.

In order to check the quality of the photometry, we compared our fluxes and equivalent widths with those taken from the literature (see Table 6). Figure 4 shows the plots of the Hα fluxes and equivalent widths reported in other works vs. ours. The linear regressions found for both plots are the following:

$$\log F(\mathrm{H}\alpha + [\mathrm{N\,II}])_{\rm this\ work} =$$

$$0.34(\pm0.91) + 1.03(\pm0.07) \times \log F(\mathrm{H}\alpha + [\mathrm{N\,II}])_{\rm literature} \quad (1)$$

$$\log EW(\mathrm{H}\alpha + [\mathrm{N\,II}])_{\rm this\ work} =$$

$$0.24(\pm0.11)+0.85(\pm0.07)\times\log EW(\mathrm{H}\alpha+[\mathrm{N\,II}])_{\rm literature}. \quad (2)$$

Both plots show a discordant point, which corresponds with galaxy CGCG 097-114. This galaxy was measured by Kennicutt et al. (1984), Moss et al. (1988), Moss et al. (1998) and Gavazzi et al. (1998). There is agreement in the flux between our data and that of Kennicutt et al. (1984) but not in the equivalent width. The measurements by Moss et al. (1988, 1998) are consistent with each other, but not with other sources. The equivalent width by Gavazzi et al. (1998) is fairly consistent with ours.

4. Discussion

4.1. The Hα luminosity function

The Hα luminosity functions were computed separately for the two clusters under study from the measured fluxes. $H_0 = 50$ km s^{-1} Mpc^{-1} is assumed to allow a direct comparison with Gallego et al. (1995).

Hα fluxes were corrected for [NII] contamination and dust extinction. The first correction is the one proposed by Gavazzi et al. (2002, in prep.), based on the relationship found between the H band luminosities and the [NII]/Hα ratio. After a empirical relationship between the H and r' magnitudes for the galaxies in common in both samples the correction was finally given by:

$$\log[\mathrm{N\,II}]/\mathrm{H}\alpha = 1.26 - 0.19 \times r' + 0.70 \times \log D \quad (3)$$

D being the distance of the galaxies in Mpc.

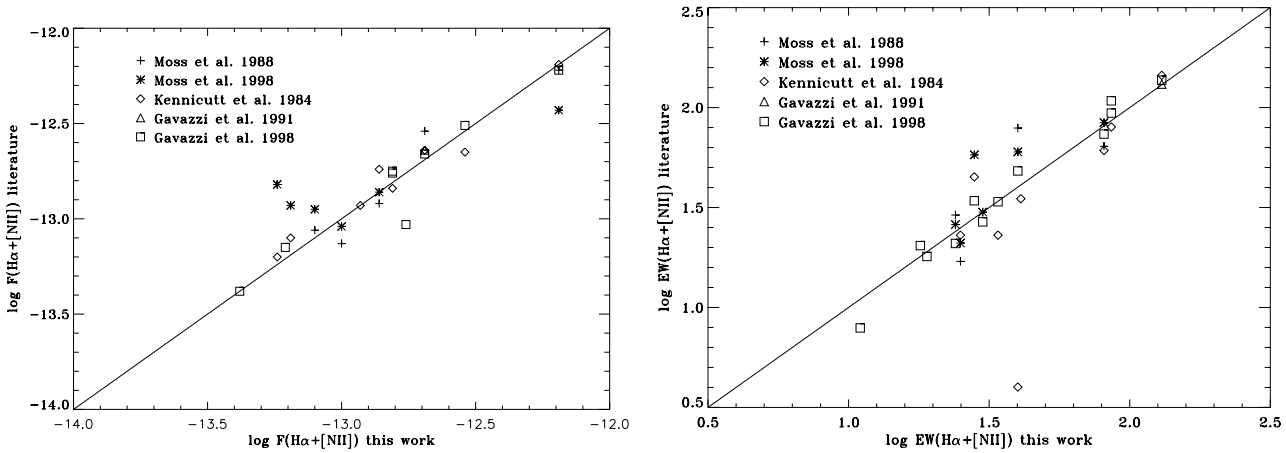

Fig. 4. Comparison between our fluxes (left) and equivalent widths (right) and the values reported in the literature for some galaxies in common. Fluxes are expressed in erg s^{-1} cm^{-2} and equivalent widths in Å.

The morphological type dependent dust extinction correction was taken from Boselli et al. (2001). For galaxies with known morphological type (from NED or other sources), the correction was taken to be

$$A(\mathrm{H}\alpha) = \begin{array}{l} 1.1 \text{ mag, for type Scd or earlier} \\ 0.6 \text{ mag, for type Sd or later.} \end{array}$$

For unclassified galaxies we adopted $M_B = -18.25$ as the statistical limiting magnitude for galaxy types intermediate between Scd and Sd, from Sandage et al. (1985).

The contribution of active nuclei to the Hα detections is negligible because no relevant point-like nuclear features were detected in the Hα frames.

In order to normalize the luminosity function to a proper volume, angular radii of 3 and 4 degrees were assumed for Abell 1367 and Coma respectively (Gavazzi et al. 1995), corresponding to linear sizes of 4.6 and 6.5 Mpc. The clusters were assumed spherically symmetric, thus the surveyed volume corresponds to the intersection between the solid angle covered by our observations and the sphere containing the clusters.

A statistical correction was applied to account for the incomplete velocity coverage of the adopted [SII] filter. Figure 5 shows the flux distribution of galaxies with known redshift versus their radial velocities. The dashed line represents the Gaussian distributions of velocities described in Sect. 2. The shaded regions correspond to the velocity ranges excluded from the filter transmitance window for each cluster. We estimate that about 20% of the velocity distribution for Abell 1367 and 11% for Coma are not within the transmitance window of the narrow band filter. We also corrected in a consistent way the effects of the velocity distribution of the Hα emitting galaxies with unknown redshift. The correction was performed as follows: first, we randomly distributed the velocities of these galaxies following the Gaussian probability density function with mean velocities and dispersions as described in Sect. 2. New Hα fluxes were derived for these galaxies, according to the values of the transmitance of the [SII] filter, for the randomly chosen velocities. If the assigned velocity

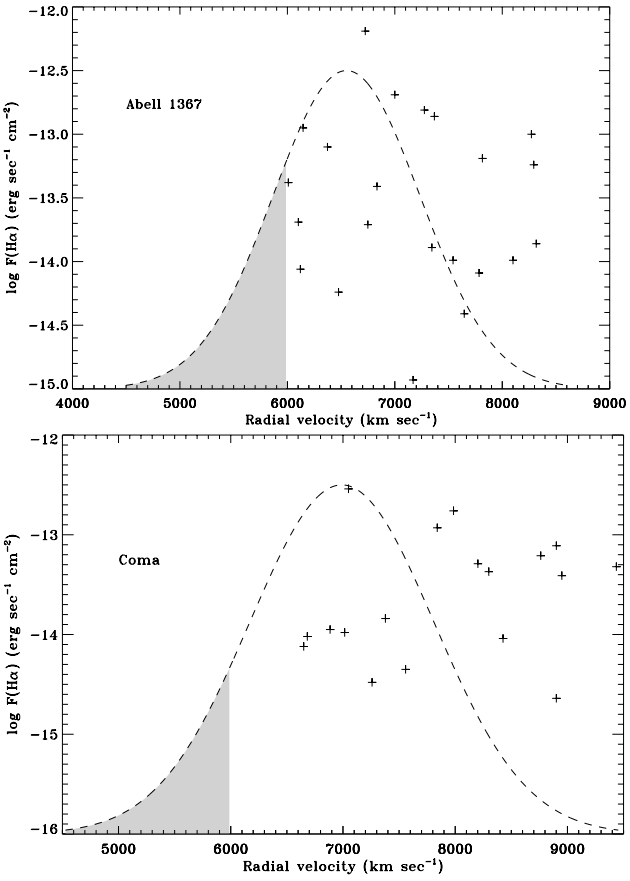

Fig. 5. Distributions of the radial velocities of the galaxies in Abell 1367 (upper plot) and Coma (lower plot). The velocity distributions of the clusters assumed Gaussians are plotted with dashed lines. The shaded regions correspond to the range of velocities not covered because of the low transmitance of the filter. Only galaxies with known redshift were included in the plots.

of any of these galaxies gave a transmitance <50%, the object was discarded. The final correction was performed by assuming that the relationship, if any, between the radial

Table 2. Counts per luminosity bin.

$\log L(\mathrm{H}\alpha)$ erg s^{-1}	Av. Number of gal. Abell 1367	Coma
38.8	8	2
39.8	18	11
40.8	13	8
41.8	1	1

velocities of the galaxies and the Hα fluxes should be symmetric with respect to the mean velocity of the cluster. We repeated this procedure ten times in order to estimate the statistical uncertainties induced by this effect on the luminosity function. Thus, Hα luminosity functions were computed with ten different flux distributions for each cluster.

The functional form assumed for the LF is the Schechter (1976) function:

$$\phi(L)\mathrm{d}L = \phi^*(L/L^*)^{\alpha}\exp(-L/L^*)\mathrm{d}(L/L^*). \quad (4)$$

The size of the bins was taken to be $\delta \log L = 1.0$ in order to minimize the statistical errors. Table 2 shows the number counts per luminosity interval for both clusters, averaged over the different random distributions of velocities for the galaxies with unknown redshift.

Table 3 lists the obtained best fitting Schechter parameters of the upper and lower envelopes for each cluster, as well as the parameters for the average LFs finally adopted.

The upper and lower envelope Hα LFs of the two clusters are given in Fig. 6. Shaded regions between the envelopes show the range of uncertainty of the Hα LF for each cluster. The points correspond to the mean values listed in Table 2, and the error bars show their typical poissonian uncertainties. As reference, we plot the Hα LFs of field galaxies obtained by Gallego et al. (1995), Tresse & Maddox (1998) and Sullivan et al. (2000). The lines are truncated at the completeness limits of each sample.

Disregarding non-completeness effects, which should only affect our lowest luminosity bins, the LFs of the two clusters are in fair agreement. The apparent difference with the field LFs is mainly in the normalization since the density of galaxies is several orders of magnitude larger

Table 3. Best fitting parameters for the upper and lower envelopes corresponding to Abell 1367 and Coma. Also, the average adopted parameters for the Hα LF are listed.

	$\log \phi^*$ Mpc^{-3}	α	$\log L^*$ erg s^{-1}
	Abell 1367		
Upper envelope	−0.06	−0.94	41.37
Lower envelope	+0.20	−0.72	41.21
Average	+0.06	−0.82	41.30
	Coma		
Upper envelope	−0.09	−0.70	41.24
Lower envelope	−0.04	−0.53	41.21
Average	−0.07	−0.60	41.23

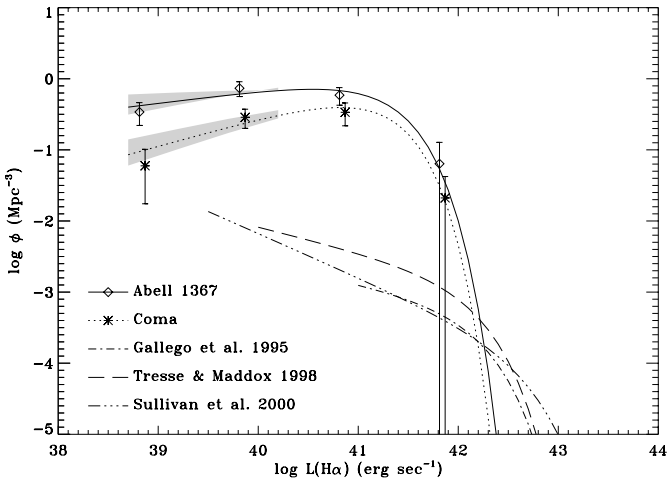

Fig. 6. Hα luminosity functions for Abell 1367 (diamonds) and for Coma (asterisks). The best fittings to Schechter functions are shown together with those found for the local Universe (Gallego et al. 1995), for $z \approx 0.2$ (Tresse et al. 1998) and for a sample of UV selected galaxies (Sullivan et al. 2000). The shaded regions show the uncertainty region between the lower and upper envelopes.

in clusters than in the field. Beside the normalization, the shape of the cluster LFs appears steeper at the bright end and flatter at the faint end. The former derives from undersampling at high luminosity (due to small volume coverage in the two clusters we do not detect any object with $F(H\alpha) \geq 10^{42}$ erg s^{-1} as opposed to Gallego et al. 1996).

The slope of the fitted LFs appear different among clusters and field at the faint end. However the data points, within the completeness limits of each survey, appear in full agreement among each other, as shown in Fig. 7.

In this figure we scaled the cluster LFs in such a way that they match the field LF at $\log L(\mathrm{H}\alpha) \approx 41$ erg s^{-1}. Above $\log L(\mathrm{H}\alpha) \approx 40$ erg s^{-1}, where all the samples are complete, there is consistency between the field and the cluster datasets. Nothing can be said for fainter luminosities because the field samples are incomplete or present rather poor statistics, opposite to the present cluster survey which is complete to $\log L(\mathrm{H}\alpha) \approx 39$ erg s^{-1}. Deeper Hα surveys of the field are necessary to assess if the differences at the faint luminosity end are significant.

4.2. The Virgo cluster

It is instructive to compare the Hα LF of A1367 and Coma with that of the Virgo cluster. Given its large angular size, performing a complete Hα survey of this cluster would be prohibitive. However Hα observations of most of the brightest galaxies (230 objects brighter than $B = 16$ mag) are available (Boselli & Gavazzi 2002; Gavazzi et al. 2002). Using these data we construct a "pseudo" Hα LF by transforming the B band LF into an Hα one after having shown that Hα luminosity and M_B are found proportional one-another.

Table 4. Some properties of the selected Hα emitting galaxies in Abell 1367.

Name	CGCG	Other	RA	Dec.	v_r	r'	F_α	Δ_f	W_α	Δ_W
114024+195747	—	—	11 40 24.90	+19 57 47.7	6749	15.48	−13.71	0.04	14	1
114038+195437	—	—	11 40 38.96	+19 54 37.4	6500††	17.35	−14.09	0.05	36	3
114107+200251	—	—	11 41 07.79	+20 02 51.3	6500†	18.91	−14.60	0.05	43	4
114110+201117	—	—	11 41 10.47	+20 11 17.7	6500†	17.57	−13.95	0.04	56	2
114112+200109	—	—	11 41 12.81	+20 01 09.9	6500†	19.44	−14.80	0.07	38	5
114141+200230	—	—	11 41 41.20	+20 02 30.5	6500†	17.37	−14.26	0.06	26	4
114142+200054	—	—	11 41 42.57	+20 00 54.9	6500†	17.33	−14.36	0.07	19	3
114149+194605	—	—	11 41 49.79	+19 46 05.1	6500†	17.52	−14.37	0.05	23	2
114156+194207	—	—	11 41 56.69	+19 42 07.8	6500†	19.77	−15.10	0.07	36	5
114157+194329	—	—	11 41 57.90	+19 43 29.4	6500†	20.21	−15.29	0.05	34	3
114158+194149	—	—	11 41 58.05	+19 41 49.6	6500†	19.46	−15.02	0.06	38	4
114158+194205	—	—	11 41 58.10	+19 42 05.9	6500†	20.30	−15.27	0.04	49	2
114158+194900	—	—	11 41 58.26	+19 49 00.9	6500†	20.70	−15.53	0.07	32	4
114202+194348	—	—	11 42 02.30	+19 43 48.5	6500†	20.83	−15.35	0.05	70	6
114202+192648	—	—	11 42 02.96	+19 26 48.2	6500†	19.54	−14.66	0.06	32	4
114214+195833	097-062	PGC 036330	11 42 14.55	+19 58 33.6	7815	14.51	−13.19	0.04	28	1
114215+200255	097-063	PGC 036323	11 42 15.70	+20 02 55.2	6102	15.36	−13.69	0.04	13	1
114218+195016	—	—	11 42 18.08	+19 50 16.1	6476	15.79	−14.24	0.04	6	1
114239+195808	—	—	11 42 39.23	+19 58 08.0	7345	16.95	−13.89	0.04	40	1
114240+195716	—	—	11 42 40.36	+19 57 16.6	6500†	17.68	−14.70	0.08	13	2
114256+195757	097-073	PGC 036382	11 42 56.67	+19 57 57.7	7275	15.50	−12.81	0.04	86	1
114313+193645	—	—	11 43 13.08	+19 36 45.8	6500††	17.27	−14.06	0.05	30	3
114313+200015	097-079	PGC 036406	11 43 13.93	+20 00 15.6	7000	16.50	−12.69	0.04	130	2
114341+200135	—	—	11 43 41.62	+20 01 35.3	6500†	17.08	−14.15	0.06	25	3
114348+195812	097-087	UGC 06697	11 43 48.59	+19 58 12.8	6725	14.22	−12.19	0.04	81	2
114348+201456	—	—	11 43 48.92	+20 14 56.0	6146	15.86	−12.95	0.04	137	1
114349+195833	—	—	11 43 49.87	+19 58 33.2	7542	16.11	−13.99	0.04	19	2
114355+192743	—	—	11 43 55.71	+19 27 43.9	6500†	18.72	−14.67	0.07	27	4
114358+201105	097-092	PGC 036478	11 43 58.17	+20 11 05.6	6373	14.71	−13.10	0.04	30	1
114358+200433	097-091	NGC 3840	11 43 58.81	+20 04 33.0	7368	13.92	−12.86	0.07	25	4
114400+200144	097-097	NGC3844	11 44 00.86	+20 01 44.5	6834	13.62	−13.41	0.04	5	1
114430+195718	—	—	11 44 30.41	+19 57 18.8	6500†	20.23	−14.38	0.04	418	19
114447+194624	097-114	NGC 3860B	11 44 47.88	+19 46 24.6	8293	15.33	−13.24	0.05	40	4
114454+194733	—	—	11 44 54.22	+19 47 33.2	6500††	20.27	−13.99	0.06	103	17
114454+194635	097-125	PGC 036589	11 44 54.99	+19 46 35.8	8271	14.50	−13.00	0.05	24	2
114454+200101	—	—	11 44 54.71	+20 01 01.5	6500††	16.17	−14.41	0.04	6	1
114503+195002	—	—	11 45 03.38	+19 50 02.7	6500†	17.90	−14.76	0.07	9	1
114506+195801	097-129E	NGC 3861B	11 45 06.91	+19 58 01.6	6009	14.64	−13.38	0.06	19	2
114513+194523	—	—	11 45 13.86	+19 45 23.0	6500††	15.60	−13.86	0.04	12	1
114518+200009	—	—	11 45 18.00	+20 00 09.5	6500†	17.54	−14.28	0.06	22	3
114603+194712	097-143B	—	11 46 03.68	+19 47 12.9	7170	15.80	−14.93	0.05	1	1

† Objects with unknown redshift but detected in the net Hα frames
†† Objects for which we have measured the redshift. It will appear in a subsequent paper.

Figure 8 shows the Hα luminosity vs. the absolute M_B magnitude relationship. Distances are estimated according to the Virgo cluster group membership, as defined in Gavazzi & Boselli (1999). The best fit to the data gives a slope of 0.37, consistent with 0.40 (i.e. a slope of 1 in a luminosity-luminosity plot). For simplicity we adopted this last value, because it allows to transform the observed B band Schechter function into an Hα LF of the same functional form. Therefore we adopt:

$$\log L(\mathrm{H}\alpha) = -0.40 \times M_B + 33.12. \quad (5)$$

Combining this relationship with the B band luminosity function for spirals and irregulars in the Virgo core obtained by Sandage et al. (1985) we obtain an Hα LF:

$$\phi'(L) = 1.07 \times (L/10^{41.2})^{-0.8} \exp[-(L/10^{41.2})]. \quad (6)$$

Figure 9 shows the Virgo Hα LF together with the ones obtained for Abell 1367 and Coma. The shaded region reflects the scatter in the relationship between Hα luminosities and M_B found in Virgo. The shape of the Virgo LF appears consistent with that of Abell 1367 and Coma, despite the different nature of the three clusters, Virgo

Table 5. Some properties of the selected Hα emitting galaxies in Coma.

Name	CGCG	Other	RA	Dec.	v_r	r'	F_α	Δ_f	W_α	Δ_W
125757+280343	—	FOCA610	12 57 57.73	+28 03 43.3	8299	15.23	−13.37	0.05	22	2
125805+281433	160-055	NGC4848	12 58 05.67	+28 14 33.2	7049	14.04	−12.54	0.05	34	2
125845+284133	—	FOCA353	12 58 45.64	+28 41 33.1	7001††	17.21	−14.02	0.06	35	5
125845+283235	—	FOCA399	12 58 45.80	+28 32 35.3	7001†	17.76	−13.83	0.04	101	4
125856+275002	160-212	FOCA600	12 58 56.55	+27 50 2.7	7378	15.12	−13.84	0.05	3	1
125902+280656	160-213	FOCA498	12 59 02.14	+28 06 56.4	9436	15.15	−13.32	0.06	28	3
125907+275118	160-219	IC3960	12 59 07.97	+27 51 18.0	6650	14.50	−14.12	0.05	2	1
125923+282919	—	FOCA361	12 59 23.13	+28 29 19.0	7001††	15.75	−13.98	0.04	10	1
130006+281500	—	FOCA371	13 00 06.42	+28 15 0.9	7259	17.04	−14.48	0.07	6	1
130037+280327	160-252	FOCA388	13 00 37.99	+28 03 27.6	7840	14.68	−12.93	0.08	41	4
130037+283951	—	—	13 00 37.24	+28 39 51.6	7001††	16.86	−14.64	0.05	6	2
130040+283113	—	FOCA242	13 00 40.75	+28 31 13.4	8901	15.80	−13.11	0.05	68	6
130056+274727	160-260	FOCA445	13 00 56.03	+27 47 27.7	7985	13.11	−12.76	0.07	11	2
130114+283118	—	FOCA195	13 01 14.99	+28 31 18.5	8426	17.02	−14.04	0.05	29	3
130125+284036	160-098	FOCA137	13 01 25.04	+28 40 36.9	8762	14.41	−13.21	0.04	18	1
130127+275957	—	GMP2048	13 01 27.17	+27 59 57.0	7558	15.64	−14.35	0.04	4	1
130128+281515	—	—	13 01 28.63	+28 15 15.9	7001†	20.41	−14.96	0.04	107	6
130130+283328	—	FOCA158	13 01 30.85	+28 33 28.0	7001††	16.76	−13.95	0.06	24	2
130140+281456	—	GMP1925	13 01 40.97	+28 14 56.6	7001†	19.33	−14.43	0.07	132	36
130158+282114	—	—	13 01 58.43	+28 21 14.8	7001†	19.81	−14.39	0.04	278	8
130212+281023	—	FOCA218	13 02 12.00	+28 10 23.0	8950	16.09	−13.41	0.05	30	2
130212+281253	160-108	FOCA204	13 02 12.55	+28 12 53.0	8177	14.93	−13.29	0.04	25	1

Table 6. Comparison of the Hα fluxes and equivalent widths with data from the literature, for the objects in common.

CGCG	This work		M88[a]		M98[b]		K84[c]		G91[d]		G98[e]	
	log F	EW	log F	EW	log F	EW	log F	EW	log F	EW	log F	EW
097-062	−13.19	28	–	–	−12.93	58	−13.10	45	–	–	–	34
097-073	−12.81	86	−12.84	–	—	—	−12.84	80	–	–	−12.76	108
											−12.75	94
097-079	−12.69	130	−12.54	—	—	—	−12.64	145	−12.64	131	−12.66	137
097-087	−12.19	81	−12.22	64	−12.43	84	−12.19	61	–	–	−12.22	74
097-092	−13.10	30	−13.06	–	−12.95	30	–	–	–	–	–	27
097-091	−12.86	25	−12.92	17	−12.86	21	−12.74	23	–	–	–	–
097-114	−13.24	40	−12.82	79:	−12.82	60	−13.20	4	–	–	–	48
097-125	−13.00	24	−13.13	29	−13.04	26	–	–	–	–	–	21
097-129E	−13.38	19	–	–	–	–	–	–	–	–	−13.38	18
160-252	−12.93	41	–	–	–	–	−12.93	35	–	–	–	–
160-055	−12.54	34	–	–	–	–	−12.65	23	–	–	−12.51	34
160-260	−12.76	11	–	–	–	–	–	–	–	–	−13.03	8
160-098	−13.21	18	–	–	–	–	–	–	–	–	−13.15	20

[a] Moss et al. (1988).
[b] Moss et al. (1998).
[c] Kennicutt et al. (1984).
[d] Gavazzi et al. (1991).
[e] Gavazzi et al. (1998).

being unrelaxed and spiral rich, Abell 1367 relaxed and spiral rich, and Coma relaxed and spiral poor.

4.3. Star formation rates in clusters

The total star formation rate per unit volume for clusters is derived by integrating the best fitting Schechter functions over the whole range of luminosities. To be consistent with Gallego et al. (1995), we convert the Hα luminosities to star formation per unit time using:

$$L(\mathrm{H}\alpha) = 9.40 \times 10^{40} \frac{SFR}{M_\odot\ \mathrm{yr}^{-1}} \mathrm{erg\ s}^{-1}. \quad (7)$$

Total integrated SFRs of 2.20 and 1.36 $M_\odot$ yr^{-1} Mpc^{-3} are obtained for Abell 1367 and Coma respectively, i.e.

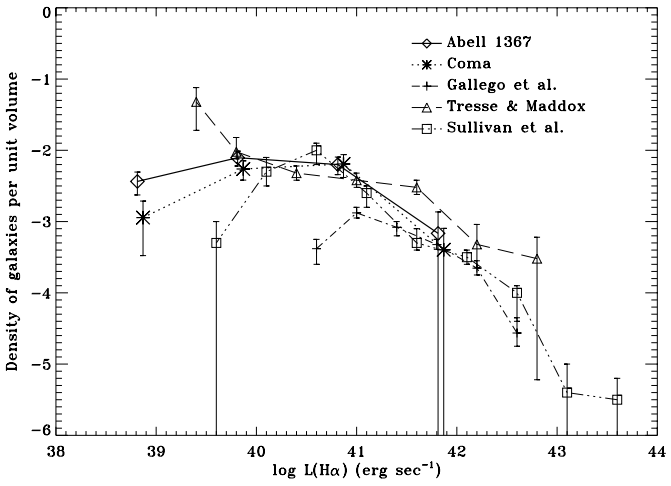

Fig. 7. Galaxy number density per unit volume vs. the Hα luminosity for the clusters and for the different field samples. The cluster counts have been normalized to properly match the field counts.

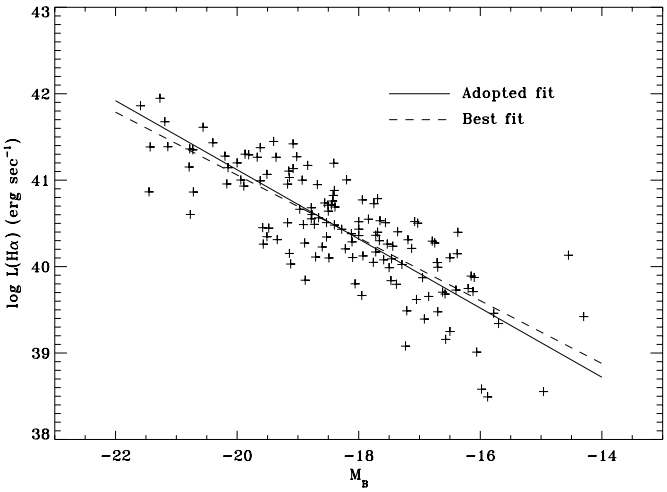

Fig. 8. M_B vs. $\log L(\mathrm{H}\alpha)$ for a large sample of Virgo galaxies. The solid line indicates the adopted fit, the dashed line shows the best fit obtained from a least squares fitting. A distance modulus of 31.7 mag was adopted to convert observed fluxes and magnitudes to luminosities and absolute magnitudes.

more than two orders of magnitude higher than the value of 0.013 $M_\odot$ yr^{-1} Mpc^{-3} reported for the local Universe by Gallego et al. (1995).

The estimate of the contribution of the clusters to the total SFR per unit volume of the local Universe, is obtained by taking into account the local spatial density of clusters. For Abell type 2 clusters, like Abell 1367 and Coma, this value was reported to be 1.84×10^{-5} Mpc^{-3} (Bramel et al. 2000), although this number is affected by large uncertainties. We conclude that the typical contribution of Abell type 2 clusters to the SFR per unit volume is about 3.3×10^{-5} $M_\odot$ yr^{-1}, that is 0.25% of the total SFR in the local Universe.

Similarly, by integrating the Virgo Hα luminosity function, we obtain a total Hα luminosity density of 1.56×10^{41} erg s^{-1} Mpc^{-3}, which gives a SFR of 1.65 $M_\odot$ yr^{-1} Mpc^{-3}. Taking into account that the Virgo cluster is classified as Abell type 1 (Struble & Rood 1982), and assuming the spatial density for clusters of this type (Bramel et al. 2000) of 8.46×10^{-4} Mpc^{-3}, we obtain that the contribution of type 1 clusters is 1.40×10^{-3} $M_\odot$ yr^{-1} Mpc^{-3}, corresponding to 10.8% of the total SFR density in the local Universe.

5. Conclusions

We have carried out an Hα imaging survey of the central 1 deg^2 of the nearby clusters Abell 1367 and Coma. Significant Hα emission is found associated with 41 galaxies in Abell 1367 and 22 in Coma. These data are used to estimate, for the first time, the Hα luminosity function of 2 nearby clusters of galaxies. These LFs are found consistent with the Hα luminosity function derived for the Virgo cluster, despite their different nature. The typical Schechter parameters: $\phi^* \approx 10^{0.00\pm0.07}$ Mpc^{-3}, $L^* \approx 10^{41.25\pm0.05}$ erg s^{-1} and $\alpha \approx -0.70 \pm 0.10$ are obtained.

The best fitting parameters of the cluster LFs are significantly different from those found for field galaxies, in particular at the faint end where the cluster slope is shallower than the extrapolated slope of the field LF. However it must be stressed that the steep slope found in the field is based on relatively high luminosity points and no data are available below $\log L(\mathrm{H}\alpha) \approx 40$ erg s^{-1} i.e. where the cluster LFs begin to flatten out. After re-normalizing the cluster data on the field ones, the two sets of data points are found consistent within the completeness limit of the field samples. Until a deeper field LF will be available it is impossible to establish whether the apparent underabundance of low luminosity objects in clusters is a real evolutionary effect or it is an artifact due to incompleteness.

By computing the total SFR per unit volume of the cluster galaxies, and taking into account the cluster density in the local Universe, we estimate that the contribution of types 2 and 1 clusters is about 0.25% and 10.8% respectively of the SFR per unit volume of the local Universe.

Acknowledgements. This research has made use of the NASA/IPAC Extragalactic Database (NED) which is operated by the Jet Propulsion Laboratory, California Institute of Technology, under contract with the National Aeronautics and Space Administration. The INT is operated on the island of La Palma by the ING group, in the Spanish Observatorio del Roque de Los Muchachos of the Instituto de Astrofísica de Canarias.

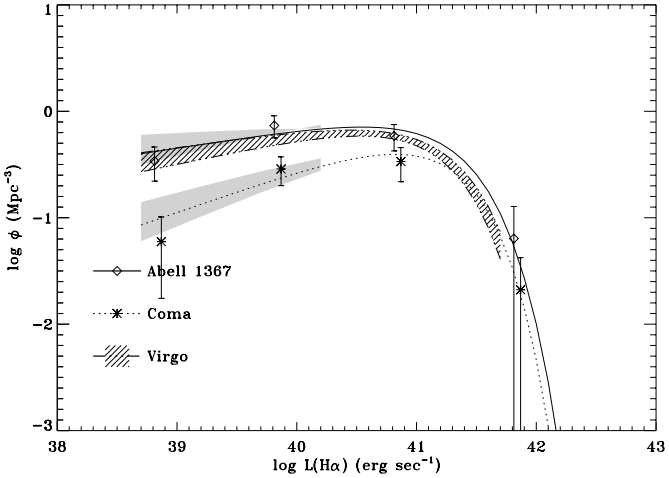

Fig. 9. Same as Fig. 6. We included the expected curve for the Virgo cluster assuming the B band luminosity function from Sandage et al. (1985) and the $L(\mathrm{H}\alpha)$ vs. M_B relationship given by Eq. (5).

References

Balogh, M. L., Schade, D., Morris, S. L., et al. 1998, ApJ, 504, L75

Bekki, K. 1999, ApJ, 510, L15

Boselli, A., Gavazzi, G., Donas, J., & Scodeggio, M. 2001, AJ, 121, 753

Boselli, A., & Gavazzi, G. 2002, A&A, submitted

Bramel, D. A., Nichol, R. C., & Pope, A. C. 2000, ApJ, 533, 601

Chincarini, G. L., Giovanelli, R., Haynes, M., & Fontanelli, P. 1983, ApJ, 267, 511

Colless, M. & Dunn, A. M. 1996, ApJ, 458, 435

Dale, D. A., Giovanelli, R., Haynes, M. P., Hardy, E., & Campusano, L. E. 2001, AJ, 121, 1886

Donas, J., Milliard, B., Laget, M., & Buat, V. 1990, A&A, 235, 60

Donas, J., Milliard, B., & Laget, M. 1995, A&A, 303, 661

Donnelly, R. H., Markevitch, M., Forman, W., et al. 1998, ApJ, 500, 138

Dressler, A. 1980, ApJ, 236, 351

Fadda, D., Girardi, M., Giuricin, G., Mardirossian, F., & Mezzetti, M. 1996, ApJ, 473, 670

Gallego, J., Zamorano, J., Aragon-Salamanca, A., & Rego, M. 1995, ApJ, 455, L1

Gallego, J., Zamorano, J., Rego, M., Alonso, O., & Vitores, A. G. 1996, A&AS, 120, 323

Gavazzi, G., & Jaffe, W. 1985, ApJ, 294, L89

Gavazzi, G., Boselli, A., & Kennicutt, R. 1991, AJ, 101, 1207

Gavazzi, G., & Contursi, A. 1994, AJ, 108, 24

Gavazzi, G., Randone, I., & Branchini, E. 1995, ApJ, 438, 590

Gavazzi, G., Catinella, B., Carrasco, L., Boselli, A., & Contursi, A. 1998, AJ, 115, 1745

Gavazzi, G., & Boselli, A. 1999, A&A, 343, 93

Gavazzi, G., Boselli, A., Mayer, L., et al. 2001, ApJ, 563, L23

Gavazzi, G., Boselli, A., Pedotti, P., Gallazzi, A., & Carrasco, L. 2002, A&A, submitted

Giovanelli, R., & Haynes, M. P. 1985, ApJ, 292, 404

Godwin, J. G., & Peach, J. V. 1982, MNRAS, 200, 733

Godwin, J. G., Metcalfe, N., & Peach J. V. 1983, MNRAS, 202, 113

Hashimoto, Y., Oemler, A. J., Lin, H., & Tucker, D. L. 1998, ApJ, 499, 589

Gunn, J. E., & Gott, J. R. 1972, ApJ, 176, 1

Haynes, M. P., Giovanelli, R., Herter, T., et al. 1997, AJ, 113, 1197

Kennicutt, R. C. 1983, AJ, 88, 483

Kennicutt, R. C., Bothun, G. D., & Schommer, R. A. 1984, AJ, 89, 1279

Merritt, D. 1983, ApJ, 264, 24

Moore, B., Katz, N., Lake, G., Dressler, A., & Oemler, A. 1996, Nature, 379, 613

Moore, B., Lake, G., & Katz, N. 1998, ApJ, 495, 139

Moore, B., Lake, G., Quinn, T., & Stadel, J. 1999, MNRAS, 304, 465

Moss, C., Irwin, M. J., & Whittle, M. 1988, MNRAS, 232, 381

Moss, C., & Whittle, M. 1993, ApJ, 407, L17

Moss, C., Whittle, M., & Pesce, J. E. 1998, MNRAS, 300, 205

Moss, C., & Whittle, M. 2000, MNRAS, 317, 667

Quinn, P. J. 1984, ApJ, 279, 596

Sakai, S., Kennicutt, R. C., & Moss, C. 2001, Am. Astron. Soc. Meet., 198, 0703

Sandage, A., Binggeli, B., & Tammann, G. A. 1985, AJ, 90, 1759

Schechter, P. 1976, ApJ, 203, 297

Schweizer, F. 1980, ApJ, 237, 303

Seguin, P., & Dupraz, C. 1996, A&A, 310, 757

Struble, M. F., & Rood, H. J. 1982, AJ, 87, 7

Sullivan, M., Treyer, M. A., Ellis, R. S., et al. 2000, MNRAS, 312, 442

Tresse, L., & Maddox, S. J. 1998, ApJ, 495, 691

Valluri, M., & Jog, C. J. 1990, ApJ, 357, 367

de Vaucouleurs, G., de Vaucouleurs, A., Corwin, J. R., et al. 1991, Third reference catalog of Bright galaxies, 1991 (New York: Springer-Verlag)

White, S. D. M., Briel, U. G., & Henry, J. P. 1993, MNRAS, 261, L8

Zwicky, F., Herzog, E., Karpowicz, M., Kowal, C., & Wild, P. 1961-1968, Catalog of Galaxies and Clusters of Galaxies, Pasadena, California Institute of Technology (CGCG)